Estimation of the Angular Variation of the Sea Surtqace Emissivity with the ATSR/ERS-1 Data

C Francois, C Ottle

REMOTE SENS. ENVIRON. 48:302–308 (1994)

Estimation of the Angular Variation of the Sea Surface Emissivity with the ATSR/ERS-1 Data

C. François and C. Ottlé**

The estimation of the sea surface temperature with a good accuracy requires precise atmospheric corrections. It also needs to take into account the variation of the surface emissivity with respect to the wavelength and to the observation angle. In this article, using the ATSR data, we evaluate the angular variation of the sea surface emissivity for viewing angles ranging between 52° and 55°. Then we compare our results with those obtained using the model of Masuda et al.

INTRODUCTION

The first European Remote-Sensing satellite, ERS-1, has been launched in July 1991. Among all the instruments carried, is the Along-Track Scanning Radiometer (ATSR). The ATSR is a passive instrument consisting of an advanced four-channel infrared radiometer providing measurements of sea surface and cloud top temperatures. This instrument was specifically designed to measure sea surface temperatures (SST) from space with an absolute accuracy better than 0.5 K.

The ATSR observes the Earth's surface along two curved swaths (about 500 km in width), one being the nadir swath (a nearly vertical path through the atmosphere), and the other the forward swath (an inclined path forward of the subsatellite point). These two views are separated by approximately 900 km in along-track distance and are almost simultaneous (the time difference is about 2 mn). The spatial resolution is about 1 km × 1 km at nadir and about 1.5 km × 2 km for the forward pixels (which is due to the viewing perspective). Further details on the scan geometry of the instrument may be found in the *ERS-1 Reference Manual* (1989) or in Prata et al. (1990).

The instrument provides fully coregistered data in four channels, at 1.6 μm, 3.7 μm, 11 μm, and 12 μm. After calibration, geometric and geolocation processing, the data processing system developed at Rutherford Appleton Laboratory (RAL, U.K.) provides two 512 km × 512 km images of the Earth's surface (the nadir view and the forward view) at these wavelengths (Eccles et al., 1989).

The estimation of SST with the accuracy needed for climate monitoring (the international TOGA program has specified an accuracy of 0.3 K; Barton et al., 1989) requires improved atmospheric correction techniques. Assuming that the atmosphere is locally stable and horizontally stratified, the dual-angle capability of the ATSR permits a more accurate atmospheric correction than what was previously possible with the other instruments. But it also requires a precise knowledge of the sea surface emissivity and of its angular behavior.

The purpose of this article is to use the dual-angle capability of the ATSR instrument to study the angular variations of sea surface emissivity (SSE). Since the same surface of the Earth is viewed under two different angles, we should be able to obtain interesting information about the directional effect of surface emissivity. In order to experimentally establish the directional nature of the surface emissivity, we perform atmospheric corrections to obtain the surface brightness temperature, which depends both on emissivity and surface temperature. Since the surface temperature remains constant between nadir and forward images, comparison of nadir and forward emissivities can be performed by comparing nadir and forward surface brightness temperatures. This enables us to show the notable variation of the emissivity for angles ranging from 0° to 55°. Then, we will determine quantitatively this angular dependence for one situation over the English Channel.

*CRPE (CNRS / CNET), Vélizy, France

Address correspondence to C. François, CRPE (CNRS / CNET), 10-12 Av. de l'Europe, 78140 Vélizy, France.

Received 3 November 1992; revised 3 April 1993.

0034-4257 / 94 / $7.00

655 Avenue of the Americas, New York, NY 10010

EVIDENCE OF THE SURFACE EMISSIVITY ANGULAR DEPENDENCE

Methodology

The radiative transfer equation gives the radiance measured by the radiometer in terms of the surface temperature T_s, the total transmittance τ_s of the atmosphere, and the surface emissivity ε_s:

$$B_\lambda(\theta,T_b) = \varepsilon_s(\theta)\tau_s(\theta)B_\lambda(T_s) + \int_{\tau_s}^{1} B_\lambda(T)\,d\tau + (1-\varepsilon_s(\theta))\tau_s(\theta)\int_{1}^{\tau_s} B_\lambda(T)\,d\tau, \quad (1)$$

where $B_\lambda(\theta,T_b)$ is the Planck function taken at the central wavelength λ, T_b is the brightness temperature measured in the same channel, and θ is the observation angle. The first term of this equation corresponds to the surface radiance, the second one is the upward atmospheric radiance, and the third term corresponds to the downward atmospheric radiance reflected by the surface up to the satellite (the surface is assumed to be a plane reflector).

Rewriting (1), while noting $a(\theta)$ for the ascending radiance and $\beta(\theta)$ for the descending radiance gives

$$B_\lambda(\theta,T_b) = \varepsilon_s(\theta)\tau_s(\theta)B_\lambda(T_s) + a(\theta) + (1-\varepsilon_s(\theta))\tau_s(\theta)\beta(\theta). \quad (2)$$

In a first approximation, the atmospheric descending radiance reflected by the surface can be neglected and if the atmospheric structure is known (the water vapor and temperature vertical profiles), one can estimate the total transmittance τ_s and the ascending atmospheric radiance $a(\theta)$ using a radiative transfer model like LOWTRAN7 from Kneizys et al. (1989), for instance. Then, we can compute $B_0(T_s)$, which is the radiance that would be emitted by the surface considered as a perfect blackbody:

$$B_0(T_s) = \frac{B_\lambda(\theta,T_b) - a(\theta)}{\tau_s(\theta)}. \quad (3)$$

Combining (2) and (3) leads to

$$B_0(T_s) = \varepsilon_s(\theta)B_\lambda(T_s) + (1-\varepsilon_s(\theta))\beta(\theta). \quad (4)$$

Therefore, comparing pixel by pixel the values of $B_0(T_s)$ calculated from the nadir view to those calculated from the forward view will be approximately the same as comparing their respective emissivities.

We have worked on one ATSR image provided by the RAL. The data have been taken on 20 September 1991 at 11 h 26 min. This image represents a rather cloudy area including Brittany (France), the English Channel, and South of Great Britain (see Fig. 1).

Atmospheric Correction with the Radiative Transfer Model LOWTRAN7

If one wants to evaluate the atmospheric effects with a radiative transfer model, the atmosphere must be precisely described. For this reason, all the radiosoundings available within this zone and at that time have been collected at the European Center for Medium range Weather Forecasts (Reading, U.K.). We have chosen the best one regarding its localization (an unclouded zone).

As has been previously explained, the scanning objective mirror of the ATSR provides two views across the subsatellite track. The zenith angle at the Earth's surface for each pixel of these images can be easily calculated and its variation is shown in Figure 2. This calculation shows that the nadir viewing angle varies from 0° to nearly 22° at the edge of the swath and that the forward viewing angle has a much lower range of variation between 52.4° and 55°.

So, by using the radiative transfer model, we have determined for the atmosphere described by the radiosonde, the whole transmittance and the upward atmospheric radiance for both spectral wave bands and for different values of the viewing angles. We have chosen five angles to calculate these quantities for the nadir image: 0°, 5°, 10°, 15°, and 20° in terms of satellite angles. We obtain thus five bands on each side of the image. We have chosen only one angle for the forward image because the atmospheric absorption shows little change in the 3° variation of the forward viewing angle.

Results

We first verified that the initial images (before the atmospheric corrections) had actually different brightness temperatures, either because of the different viewing angles or the different channels used.

Figure 3a shows the comparison on a pixel basis between brightness temperatures measured at 11 μm (Channel 3) and those measured at 12 μm (Channel 4). Figure 3b compares the temperatures measured at nadir with those measured on the forward scan. Indeed, we notice that the brightness temperatures are larger on the nadir image than on the forward image: This illustrates the smaller thickness of atmosphere to be gone through and the fact that the mean atmosphere temperature T_a remains generally smaller than the surface temperature T_s. The temperatures are also larger on the Channel 3 image than on the Channel 4 image because of the greater atmospheric transparency in this band.

Very scattered points appear on the graph comparing the nadir and the forward images (Fig. 3b) but not on the graph comparing the Channel 3 and the Channel 4 images (Fig. 3a). This is easily understood: Although both nadir and forward images have been taken simultaneously, clouds do not occupy the same location on the images because of the difference of viewing angle. For instance, a point may be under a cloud on an image and over the sea on the other, and thus appears isolated on the graph. This phenomenon does not occur when comparing images taken with the same viewing angle.

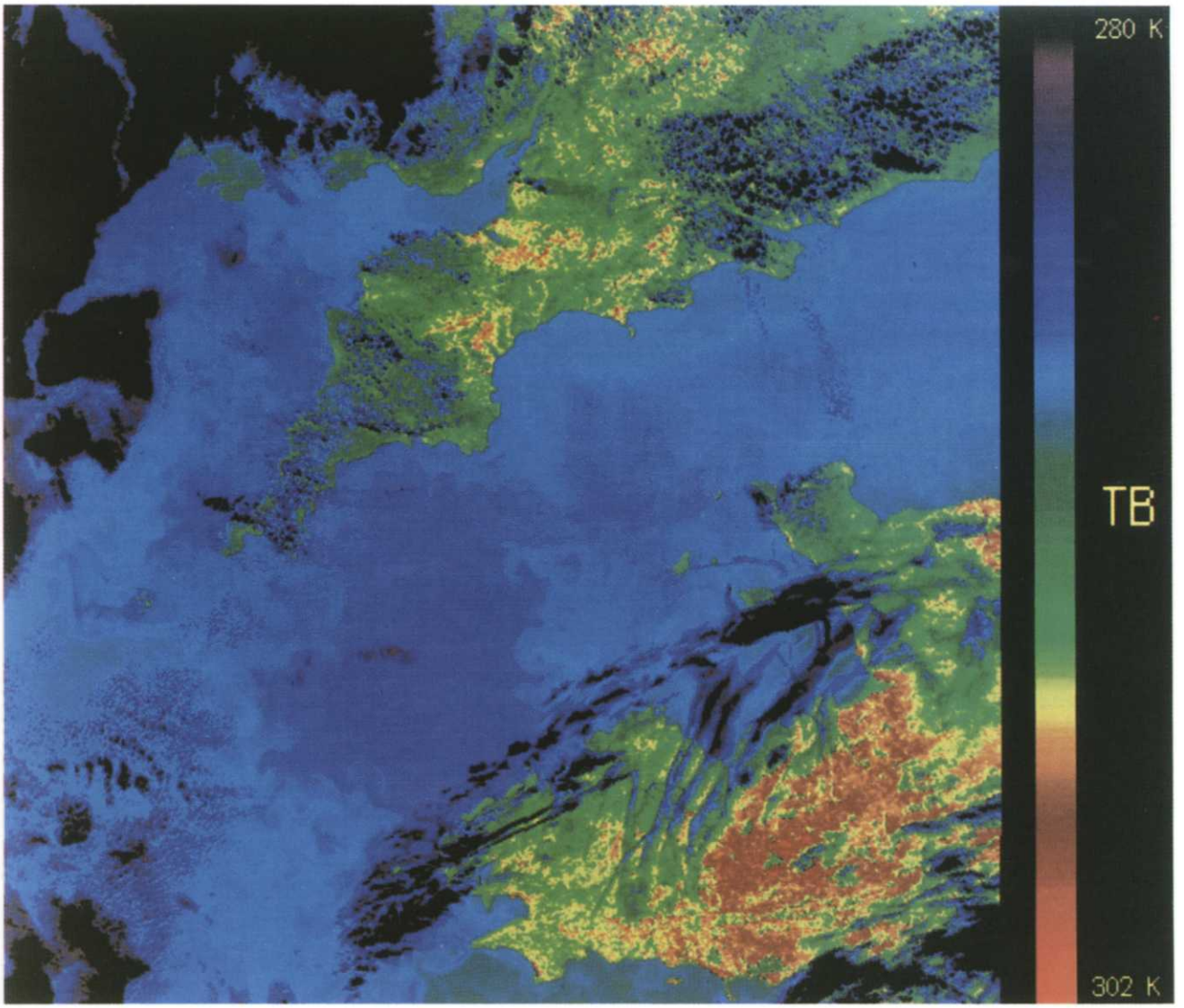

Figure 1. Surface brightness temperatures measured in the 11-μm channel at nadir.

Figure 2. Variation of the zenithal angle for both nadir and forward images with the across-track distance.

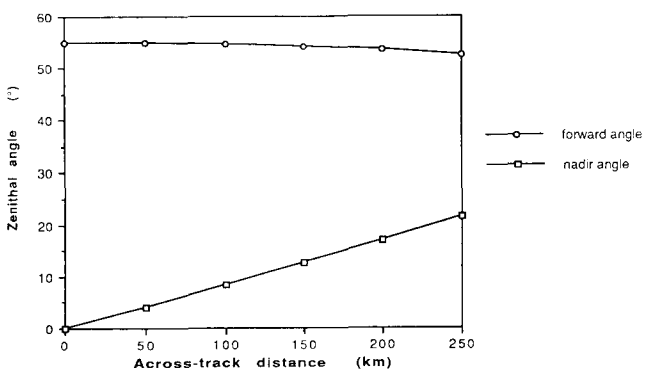

After atmospheric corrections [using Eq. (3)], we obtain the so-called surface brightness temperature T_{sb}, which verifies that $B(T_{sb})$ equals $B_0(T_s)$. Figures 4a and 4b show comparisons between the surface brightness temperatures. The scale has been limited to temperatures between 280 K and 310 K (colder temperatures correspond to cloudy pixels). In fact, points with a temperature lower than 288 K are all cloudy. Between 288 K and 292 K we observe almost only sea points, and above 292 K we find land points. But these categories are not perfectly separated, which is principally due to the cloudy or partly cloudy zones, where the temperature varies mostly continuously, whatever the soil type.

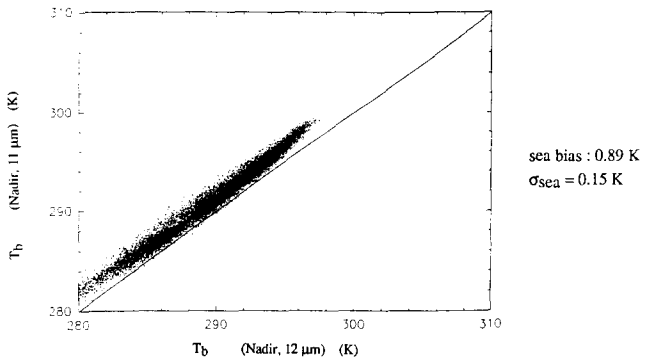

Figure 3a. Comparison of the satellite brightness temperatures measured at nadir in the 11-μm and 12-μm channels.

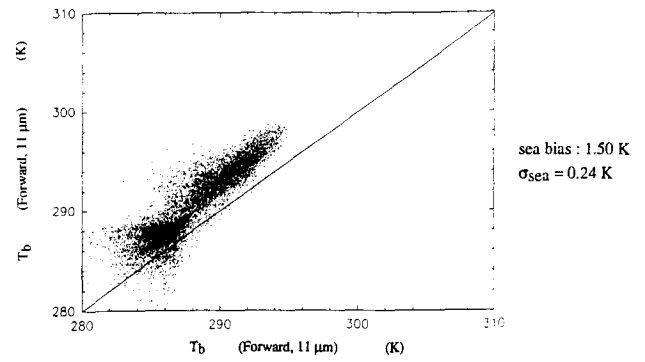

Figure 3b. Comparison of the satellite brightness temperatures in the 11-μm channel for nadir and forward views.

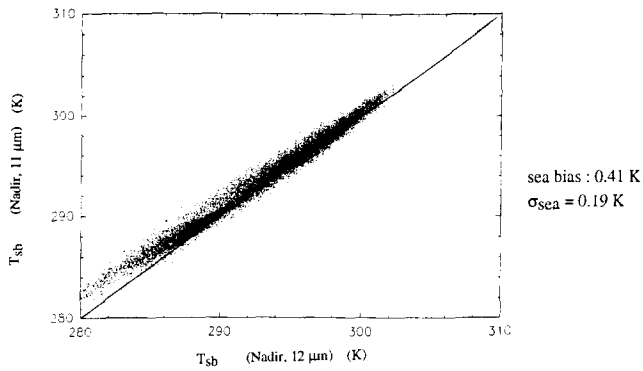

Figure 4a. Comparison of the surface brightness temperatures measured at nadir after atmospheric corrections, in the 11-μm and 12-μm channels.

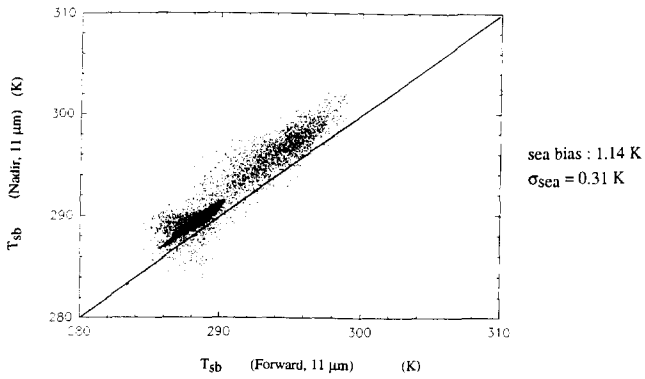

Figure 4b. Comparison of the satellite brightness temperatures measured after atmospheric corrections for nadir and forward views.

If there were no angular dependence (respectively spectral dependence) of the emissivity, we should obtain for a given pixel almost the same surface brightness temperature for both nadir and forward images (respectively both channels) [see Eq. (4)]. We can see on these figures that we actually do not obtain for the same pixel the same surface brightness temperature. More precisely, there is a bias of 1.14 K when comparing nadir and forward sea pixels (see Fig. 4b). Assuming that the radiative transfer is well described by the LOWTRAN7 model, we show here that the nadir and forward surface brightness temperatures are not equal and depend actually on the viewing angle of the pixel, that is, that the surface emissivity, for a given pixel, varies with the viewing angle.

On the other hand, the emissivity seems to vary quite less between two different channels since the surface brightness temperatures are nearly equal between the 11-μm and the 12-μm nadir images (Fig. 4a). The bias is only equal to 0.41 K, but the spectral behavior of the emissivity will not be developed here.

ANGULAR DEPENDENCE OF SURFACE EMISSIVITY

Methodology

If we come back to the radiative transfer equation without neglecting now the reflected downward radiance, we can write Eq. (4) for both paths, using the subscripts n and f, respectively, for nadir and forward terms (now we only consider the 11-μm channel):

$$[B_0(T_s)]_n = \varepsilon_s(\theta_n)B_\lambda(T_s) + (1 - \varepsilon_s(\theta_n))\beta(\theta_n), \quad (5)$$

$$[B_0(T_s)]_f = \varepsilon_s(\theta_f)B_\lambda(T_s) + (1 - \varepsilon_s(\theta_f))\beta(\theta_f). \quad (6)$$

It may be seen that the emissivity ratio is not directly available, for it depends notably on the descending radiance and also on the emissivity itself. Therefore, it turns out that the ratio $\varepsilon_s(\theta_n) / \varepsilon_s(\theta_f)$ cannot be calculated directly since $B_\lambda(T_s)$ remains unknown. On the other hand, if we suppose one of both emissivities (the nadir emissivity, for instance) to be known, we can calculate the other one using the following equation:

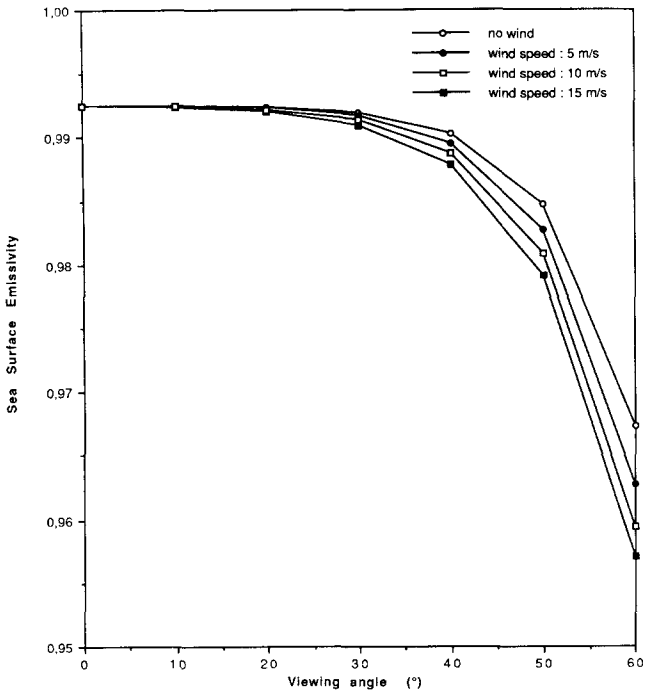

Figure 5. Variation of the modelised emissivities with the viewing angle, for different values of the surface wind speed (Masuda et al., 1988).

$$\varepsilon_s(\theta_f) = \frac{[B_0(T_s)]_f - \beta(\theta_f)}{B_\lambda(T_s) - \beta(\theta_f)}, \qquad (7)$$

where $B_\lambda(T_S)$ is deduced from (5) and the descending radiances have been calculated with LOWTRAN7.

Thus, if one of both emissivities can be prescribed to a known value, the other one can be calculated. For this purpose, we have looked to the results of Masuda et al. (1988). Using a statistical modelisation of the sea surface, the authors have tabulated the emissivity of sea water in the infrared window region as a function of the zenith angle of the observed radiation and of the surface wind speed.

Figure 5 shows the computed sea surface emissivities for a 11-μm as a function of the observation zenith angle for different values of the surface wind speed. It may be seen that for viewing angles lower than 15°, whatever the wind speed is, the emissivity is equal to 0.9925.

We know that for a nadir image the viewing angle reaches 20° at the sides of the swath, but according to Masuda's tables the emissivity would not vary much and at worst, with a 15 m / s wind, would decrease to 0.9920 for θ equal to 20°. On the other hand, things are different for angles corresponding to the forward image. First, the emissivity decreases here significantly, and most of all, even if the zenith angle at the Earth's surface does not vary much (it ranges between 52° and 55°), the emissivity varies very rapidly in this interval, and especially for high wind.

According to these results, we have chosen to fix the emissivity of the sea pixels on the nadir view and to calculate the corresponding emissivity on the forward image.

Application to the Emissivity Study on the Nadir and Forward Images

From the emissivity values modelized by Masuda et al. (1988), it appears necessary to split each image into north / south bands corresponding to different viewing angles. We have taken again the five bands we used with LOWTRAN7 for the nadir image. The selection of the noncloudy sea points has been achieved by requiring their surface brightness temperatures to be contained between 288 K and 292 K and applying a mask on the continental regions.

To obtain forward emissivities on these five bands on the forward image, we have set the nadir emissivity to 0.9925, and the mean forward emissivity has been calculated on each zone through Eq. (7). The obtained values are presented in Table 1, and Figure 6 shows the comparison with Masuda et al.'s (1988) predictions for different values of the surface wind speed. Let us note that the emissivities that we have obtained are mean values on each zone (with a standard deviation of about 10^{-3}), but all calculations were done pixel by pixel. The principal result is that the forward emissivity variation is in agreement with what we expected, that is, a decrease of the emissivity when the viewing angle increases. Moreover, the obtained values correspond in Masuda's table to an SSE modelized for a surface wind speed of about 10 m / s. This can be compared to *in situ* measurements made with two buoys situated near the French coast, giving 6 m / s and 9 m / s at the same time. The fact that the third term (β) of the radiative transfer equation is calculated for a plane surface and not a rough surface may explain these differences.

In order to get more information about the dependence of the atmospheric corrections on the retrieved forward emissivities, a sensivity test has been performed

Table 1. Retrieved Mean Forward Emissivities on Each Zone (and Corresponding Standard Deviation)

Zone	*Nb*[a]	ε_f	σ
1	7,120	0.9684	2.4×10^{-3}
2	10,309	0.9695	2.3×10^{-3}
3	2,765	0.9705	1.3×10^{-3}
4	11,356	0.9735	3.3×10^{-3}
5	1,125	0.9763	2.5×10^{-3}

[a] *Nb* = number of selected sea points for each zone.

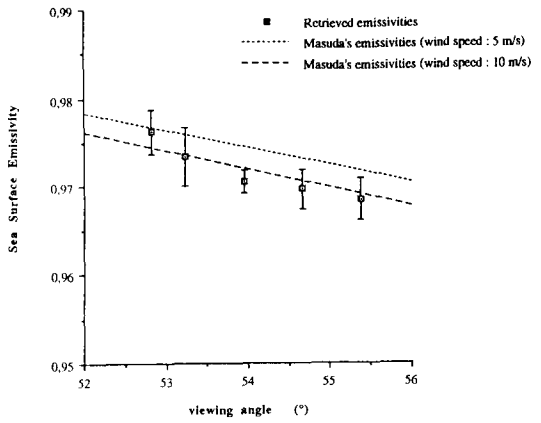

Figure 6. Comparison between the retrieved sea surface emissivities and Masuda's modelized emissivities.

by introducing into our radiosounding a noise level of 1 K in the dew point temperatures (this value is the standard deviation observed for midlatitude atmospheres and stable situations over zones of comparable size; Ottlé and Vidal-Madjar, 1992). The results show that the retrieved emissivities are normally distributed about the noiseless emissivity with a standard deviation of 7.4×10^{-4}. Since the standard deviation for the mean retrieved emissivity is about three times greater, it may be concluded that the results are not much influenced by the fact that only one radiosounding was chosen to perform the atmospheric corrections on the whole image.

The sea emissivities that we have calculated enable us to correct the surface brightness temperatures in order to obtain true surface temperatures, which are now to be equal on both images (at least for sea points, with the limitation that the SSE values which we use are only mean values). Equations (5) and (6) allow us to correct the brightness radiances in terms of the emissivities and of the descending radiances. The results are presented on Figure 7. The mean difference between the two retrieved surface temperatures is actually reduced on the sea points to about 0.05 K, with a mean standard deviation of about 0.30 K. This error is only due to the fact that we used mean values for the SSE and it can be interpreted as a measure of the error made on the SST when assuming the SSE to be constant on the north / south bands.

CONCLUSION

Using the dual-angle capability of the ATSR instrument and prescribing the surface emissivity for low values of the observation angles (less than 20°), we have calculated the sea surface emissivity for observation angles around 50°.

Figure 7. Comparison of the surface temperatures (K) at 11 μm between nadir and forward views after atmospheric and emissivity corrections.

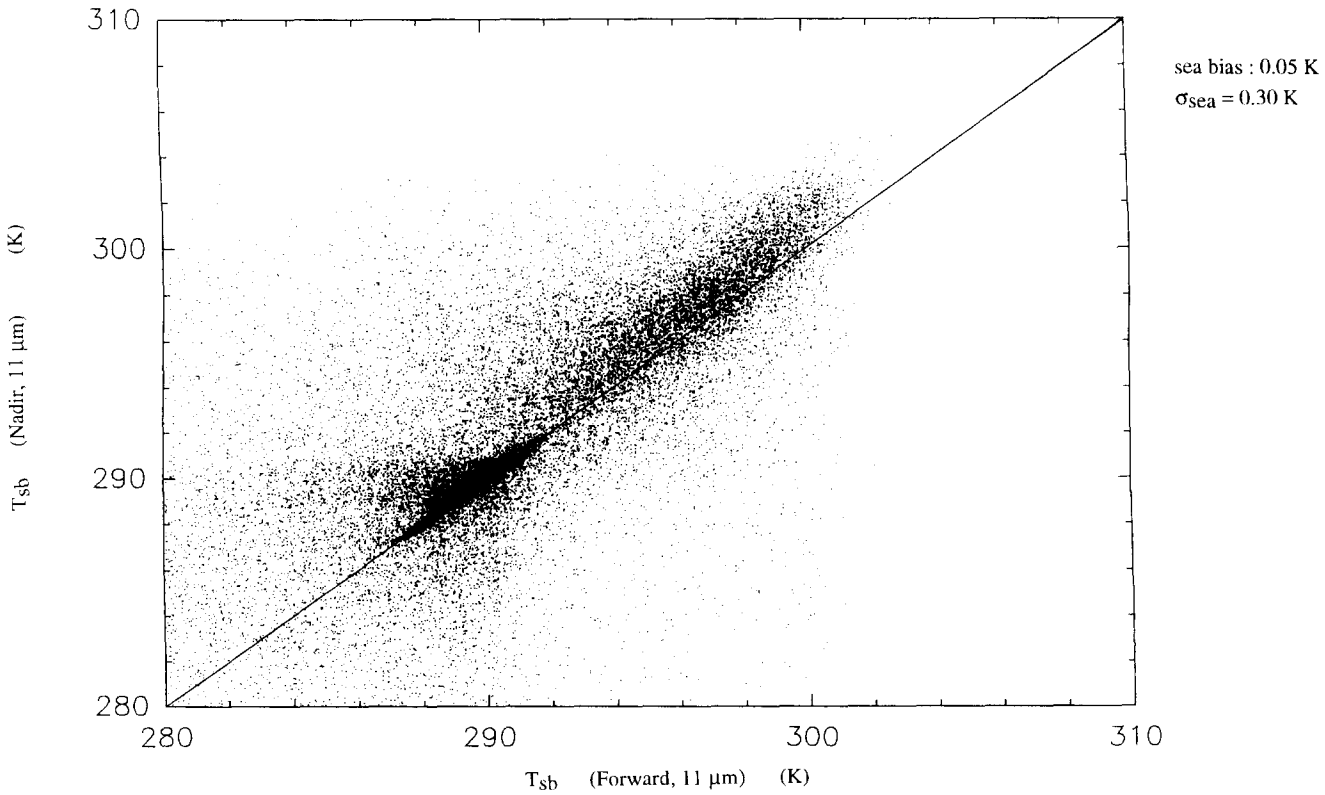

These very preliminary results show the evidence of the angular variations of sea surface emissivity and the necessity of taking it into account to obtain accurate sea surface temperatures. It has been shown that for observing angles greater than 50°, the emissivity is at least 2% lower. If neglected, such an error on SSE will lead to an error of about 1.2 K on SST.

To achieve this work, we have been obliged to perform atmospheric corrections. This was done with data from radiosondes and a radiative transfer model. Thus, we have assumed the representativity of the radiosounding on all the English Channel, although the atmospheric situation was relatively unstable in this case. Our results depend also on the assumption that the nadir SSE is known.

Given the importance of SSE for the determination of SST, it is now important to have more information on its angular and spectral variations to validate the modelizations. We have shown here a way of using the ATSR to obtain new informations on SSE, but further studies have to be done taking into account surface parameters like wind speed estimations at a comparable spatial scale.

We are grateful to the Rutherford Appleton Laboratory for providing us the ATSR data and specially to Marc Gorman and Albin Zavody for their assistance. The authors want also to thank Daniel Vidal-Madjar for fruitful discussions, Luc Tabary for his help when using the ECMWF's archiving dataset, and finally Philippe Olivier for his assistance on the image processing system.

REFERENCES

Barton, I. J., Zavody, A. M., O'Brien, D. M., Cutten, D. R., Saunders, R. W., and Llewellyn-Jones, D. T. (1989). Theoretical algorithms for satellite-derived sea surface temperatures, *J. Geophys. Res.* 94:3365–3375.

Eccles, D., Gorman, M., Lee, D., Moffat, P., and Zavody, A. (1989), Overview of the ATSR-IR off-line data processing system, internal note, Rutherford Appleton Laboratory, U.K.

ERS-1 Reference Manual (1989), DC-MA-EOS-ED-0001, ESA.

Kneizys, F. X., Shettle, E. P., Abreu, L. W., et al. (1989), Atmospheric transmittance / radiance: the LOWTRAN 7 model.

Masuda, K., Takashima, T., and Takayama, Y. (1988), Emissivity of pure and sea waters for the model sea surface in the infrared window regions, *Remote Sens. Environ.* 24:313–329.

Ottlé, C., and Vidal-Madjar, D. (1992). Estimation of land surface temperature with NOAA9 data, *Remote Sens. Environ.* 40: 27–41.

Prata, A. J. F., Cechet, R. P., Barton, I. J., and Llewellyn-Jones, D. T. (1990), The along track scanning radiometer for ERS-1—scan geometry and data simulation, *IEEE Trans. Geosci. Remote Sens.* 28:3–13.